IOP Publishing Measurement Science and Technology
Meas. Sci. Technol. **27** (2016) 025015 (6pp) doi:10.1088/0957-0233/27/2/025015

Height control for small periodic structures using x-ray radiography

M Schüttler[1,2], P Meyer[2], F Schaff[1], A Yaroshenko[1], D Kunka[2], H Besser[3], F Pfeiffer[1,4] and J Mohr[2]

[1] Lehrstuhl für Biomedizinische Physik, Physik-Department & Institut für Medizintechnik, Technische Universität München, 85748 Garching, Germany
[2] Karlsruhe Institute of Technology, Institute of Microstructure Technology, Hermann-von-Helmholtz-Platz 1, 76344 Eggenstein-Leopoldshafen, Germany
[3] Karlsruhe Institute of Technology, Institute for Applied Materials, Hermann-von-Helmholtz-Platz 1, 76344 Eggenstein-Leopoldshafen, Germany
[4] Institut für diagnostische und interventionelle Radiologie, Klinikum rechts der Isar, Technische Universität München, 81675 München, Germany

E-mail: markus.schuettler@tum.de

Received 1 September 2015, revised 14 December 2015
Accepted for publication 17 December 2015
Published 11 January 2016

Abstract

We report on a method to characterize the height of periodic x-ray absorbing structures. Such structures are used for example in grating-based x-ray interferometry. In contrast to other techniques, our approach allows for a non-destructive determination of the height based on a few transmission measurements. It can be used with conventional laboratory-based x-ray setups and is therefore of great interest at the application sites of the structures, as it allows further characterization without the need of additional hardware. Here we present the principle of the method, show first results acquired with an absorption grating and compare them with theoretical calculations and those obtained using a destructive method.

Keywords: radiography, medical imaging, microstructures, x-ray gratings, height measurement, phase-contrast

(Some figures may appear in colour only in the online journal)

1. Introduction

Grating based x-ray phase-contrast and dark-field imaging (XGI) is a promising imaging technique developed in the last decade [1–4]. The main advantage of XGI is the acquisition of complementary contrast modalities in addition to the absorption signal, as provided by conventional x-ray imaging. These modalities are currently explored both in biomedical imaging, as well as in material science [5, 6]. The first additional modality, obtained with differential phase-contrast (DPC), provides an improved soft tissue contrast, which is typically an issue of standard absorption based x-ray imaging [7–10]. The so-called dark-field contrast (DFC) is sensitive to the scattering of x-rays by small structures in the sample and thereby reveals completely new diagnostic possibilities, by providing morphological information well below the resolution limit of conventional x-ray detectors [11–14].

The three-grating Talbot–Lau interferometer is the most common setup for acquisition of differential phase-contrast and dark-field images. It consists of a source grating which provides sufficient lateral spatial coherence, a phase grating, which creates an interference pattern and an analyzer grating to retrieve the signal from this interference pattern. The latter is necessary due to the large pixel size of conventional x-ray detectors.

The source grating and the analyzer grating both are absorption gratings with periodic absorbing structures. A high transmission difference between grating lamellae and gaps is necessary to achieve proper image quality. Therefore the grating lamellae are commonly made out of high absorbing materials such as gold, while the spaces between are either empty or filled with the material used as a template for the metal deposition. In order to maximize the performance of a given setup, the transmission of x-rays through the grating

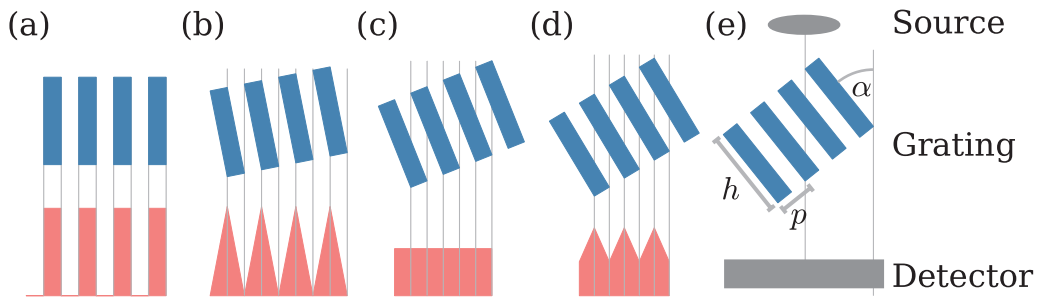

Figure 1. Periodic structures with a duty-cycle of 0.5 and an aspect ratio of 5 with different rotation angles. In (a)–(d) their respective projected height profiles are shown underneath. (e) Sketch of the experimental setup. The grating is placed in between the x-ray source and the detector on a rotation stage. (a) Case of illumination parallel to the lamella. (b) With increasing rotation the case described by (1) with $n = 0$ is observed and the projected height shows a triangular shape. (c) Further rotation leads to a flat profile as indicated in (2) with $n = 1$. (d) Subsequent tilting produces a higher order of triangular profiles.

lamellae should be as low as possible. For example, with an x-ray energy of 50 keV, gold structures of 218 μm height are required to achieve 5% transmission. For a typical grating period of 4.8 μm this results in an aspect ratio of almost 100. While other methods exist [15] for lower aspect ratios, such high aspect ratio gratings are today fabricated only by the LIGA process [16, 17].

This process is a sophisticated chain of micro-structuring techniques. During the last steps, gratings are fabricated by electrodeposition of gold in a polymer matrix patterned by deep x-ray lithography. The progress of the metal deposition is controlled by monitoring the deposited charge. As the amount of charge directly translates to the gold volume, knowledge of the exposed area allows to calculate the deposited height. The area, however, varies with the width of the lamellae, a parameter that is hard to control due to tolerances of resist properties and the influence of exposure conditions. This often leads to deviations from the design height. In addition, for such small structures, the deposition speed is also not uniform over the whole grating area, which leads to local variations of the grating height.

The actual height of the grating is of great interest, as it is an important factor for the performance of the grating. Height deviations decrease setup performance. Too high grating structures reduce the field of view due to shadowing effects. They occur when the beam hits the side areas of the grating under an angle. Lack of height of gratings result in deteriorated DPC and DFC signals as the grating transmits a high background. Therefore, knowledge of the grating height is important to correctly assess and optimize setup performance on the one hand, and on the other hand it will help to improve the electroplating process.

Existing methods for determining the height of the gratings are either destructive or difficult to implement. Destructive methods are based on evaluation of grating cross sections, either by removing part of the grating structures via ablative laser (see section 3) or ion beams or by simply breaking or cutting the substrate. Measurements with stylus instruments are difficult as the polymer matrix is usually kept between the lamellae and therefore no reference is available in close proximity to the grating structures. Furthermore, reference structures next to the grating are not reliable due to the inhomogeneity of the electroplating. The substrate itself might additionally contribute to height variations. Directly measuring the absorption of the grating lamellae and using the Beer–Lambert law to calculate the height would require exact knowledge of the x-ray spectrum of the source as well as the material parameters.

In order to overcome these limitations we propose a new technique to characterize the height of periodic grating structures in a conventional lab based x-ray setup.

2. Materials & methods

2.1. Height analysis

Ideal absorbing grating lamellae have rectangular shape with non-absorbing spaces in between. The width of the structures is the period p of the grating times the duty-cycle DC of the structure. We assume the height h to vary only slowly over the complete grating area. Therefore we assume the height of a series of neighboring structures to be constant. Under illumination in parallel beam geometry and perpendicular to the surface, i.e. $\alpha = 0$, the projected height profile of the periodic structure consequently is a series of boxcar functions (figure 1(a)). When α is increased and the structure is tilted this profile changes to a trapezoidal shape, until the diagonal of the rectangles is parallel to the beam and the height profile becomes a triangular function at an angle that is found to be

$$\alpha_{\triangle,n} = \tan^{-1}\left((n + DC)\frac{p}{h}\right), \tag{1}$$

where $n \in \mathbb{N}_0$ represents the order of the extremum. $n = 0$ is the first occurrence of a triangular shape, as shown in figure 1(b). A further increase of the tilt angle leads to a flat height profile, when the bottom corner of a grating bar lines up with the respective corners of the next grating bar at

$$\alpha_{\square,n} = \tan^{-1}\left(n \cdot \frac{p}{h}\right), \tag{2}$$

where $n = 1$ represents the first flat projected height profile, corresponding to figure 1(c). Further tilting yields additional repetitions of these patterns. The corresponding angles can be found by increasing n in (1) and (2). Using this derivation for the shape of the projected height, it is possible to calculate

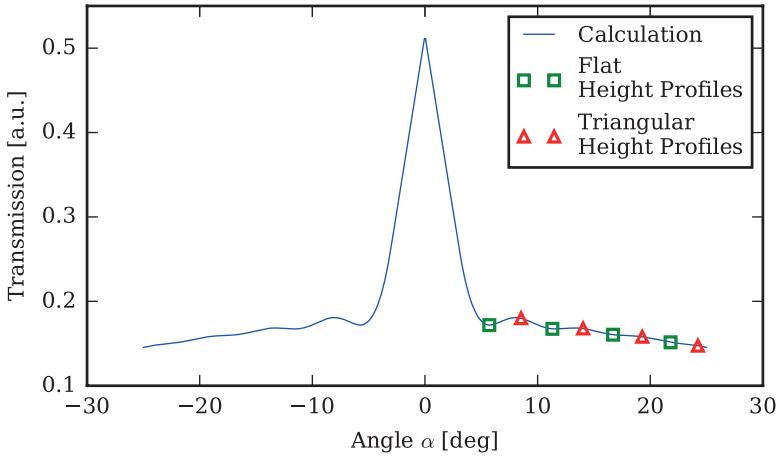

Figure 2. Calculated intensity curve for a periodic structure of 100 μm height, 10 μm period and duty-cycle 0.5. The absorbing material was gold and the x-ray energy is 35 keV. Thus, the maximum relative transmission is slightly above 0.5 due to the *DC* of 0.5 and the non-perfect absorption. The respective markers indicate the theoretical transmission values for the angles of flat and triangular height profiles according to (1)–(4). The angles of the local maxima deviate slightly from the angles of triangular height profiles. The minima, however, closely match the positions of flat height profiles.

the transmission functions for the cases of flat and triangular shapes as

$$T_{\square,n} = \exp\left(\frac{-\mu h}{2\cos\alpha}\right) \tag{3}$$

and

$$T_{\triangle,n} = \frac{(2n+1)\cos\alpha}{\mu h}\left(\exp\left(\frac{-\mu h}{\cos\alpha}\cdot\frac{n+1}{2n+1}\right) - \exp\left(\frac{-\mu h}{\cos\alpha}\cdot\frac{n}{2n+1}\right)\right), \tag{4}$$

where μ is the attenuation coefficient of the absorbing material.

Figure 2 shows the calculated transmission of the grating structures as a function of the rotation angle α. The average absorber thickness increases with $1/\cos\alpha$ and therefore the measured average intensity behind the grating decreases with α. However, due to the described behavior of the projected structure height under rotation and the exponential decrease of transmission with absorber thickness, there are deviations from the $1/\cos\alpha$ curve. The maximum deviations will be found near the angles that produce a triangular height profile. The position and shape of the local maxima depend on the height, the period and the duty cycle of the structures (see (1)). However, the transmission minima found between two maxima only depend on the height and period of the structure (see (2)). Thus, we can calculate the height of the structure if the period and minima positions are known.

2.2. Theoretical Calculations

While the direct calculation of angles and transmissions for distinct shapes, such as flat and triangular height profiles is possible, the calculation for arbitrary height profiles is not straightforward. Therefore, we performed calculations to verify our method and acquire theoretical intensity values for all rotation angles. In order to do this, we implemented an algorithm, which calculates the effective x-ray path length through the absorber material depending on the parameters of the structure (h, p, DC), the incidence angle of the x-ray beam and the relative position of the beam in the structure. The absorber length and the according transmission are calculated for multiple parallel beam positions along one period of the structure. The transmission is then averaged over the length of the period. A numerically derived transmission curve obtained by performing the calculations for every angle is presented in figure 2.

The comparison between the theoretical values provided by (1)–(4) and the numerical values present a very good agreement. It becomes apparent however, that the positions of the peak maxima do not line up with the angles of triangular height profiles. The minima, on the other hand, align well with the positions predicted by (2). Figure 3 shows the dependence of the peak shape on the duty-cycle of the structure. As predicted by (1)–(2), the maxima of transmission shift, while the minima remain stationary.

2.3. Experimental setup

In order to confirm the calculation results, experimental measurements were performed with a laboratory CT-setup using an x-ray WorX (Garbsen, Germany) SE 160 tube with a tungsten reflection target. The source was operated at 60 kVp and 0.67 mA, resulting in a tube power output of 40 W. The images were acquired with a Varian (Palo Alto, USA) PaxScan 2520D flat panel detector with a pixel size of 127 μm × 127 μm and an active area of 19.0 cm × 23.8 cm. The sample was mounted on a Huber (Rimsting, Germany) Eulerian Cradle at a distance of 77.8 cm from the source and 116.5 cm from the detector. The investigated grating was an absorption grating with a period of 4.8 μm, a duty-cycle of 0.55 ± 0.02 and a design height of 120 μm. The grating had an active area of 5 cm × 5 cm. A sketch of the setup is presented in figure 1(e).

2.4. Data acquisition

A series of projection images was acquired while rotating the grating around the axis parallel to the grating lines.

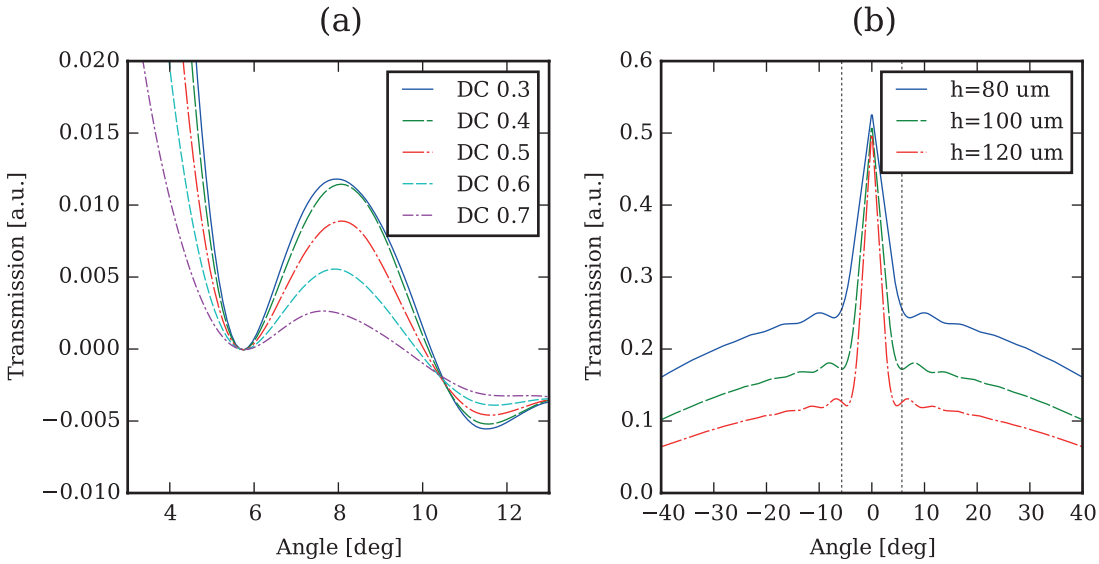

Figure 3. (a) Calculated intensity curves for periodic structures of 100 μm height, 10 μm period and duty-cycles of 0.3–0.7 as a function of the rotation angle. The transmission values (*y*-axis) of the first minima were all shifted to 0 for easier comparison. A duty-cycle of 0.5 shows the maximum at the largest angle, while deviations shift the peak to smaller angles. The minima on the contrary remain stationary. (b) Calculated intensity curve for periodic structures of 10 μm period, duty-cycle 0.5 and 80 μm, 100 μm and 120 μm height. The position of the first minimum of the 100 μm structures is marked by a vertical line. With increasing height and aspect ratio of the structures, the peaks shift closer together as predicted by (1)–(2).

The angular range of the acquisition was ±20° with a resolution of 6 images per degree, resulting in 240 total projections. Additionally, two flat-field images without sample were taken at the beginning of the scan for the background correction. The integration time of the signal was 4 s, adding up to a scan time of 16 mins.

2.5. Data processing

The processing of the data was performed using an algorithm implemented in Python (Version 2.7). For the evaluation of our method we chose a 1 mm × 1 mm region of interest (ROI) near the center of the grating. For the ROI the average intensity was extracted from the projection images after performing a flat-field correction. To correct for intensity fluctuations over the course of the scan, a relative intensity was calculated for each image and used for normalization. The relative intensity was acquired by taking the average signal of an area of the detector that was not covered by the grating or other parts of the setup and dividing by the equivalent value of the flat-field images. The intensity curve was then filtered and smoothed to facilitate the detection of the minima. After detection of the extrema, the theoretical positions of the minima were fitted to the detected positions. The effects of filtering and smoothing have been evaluated by comparing the input height of a theoretical intensity curve and the analysis result of the same curve after processing; this gives an acceptable difference of less than 4% (3.5 μm).

3. Results

Both, the experimentally measured and the calculated intensity curves are shown in figure 4. The theoretically predicted peak positions agree very well with the measured ones. The first two orders of minima allowed for a stable fit of the theoretical minima positions to the measured data. The fit results in a height of 105 μm with a standard deviation of 1.3 μm. While this height is slightly below the design height of 120 μm, variations of this order are not uncommon during the electroplating.

The differences in shape between the measured and predicted curve in the region of the primary peak might be caused by small scale variations of the grating height, which are below the resolution limit of the setup and not considered by the theoretical calculations. Such variations are commonly observed during scanning electron microscopy (SEM) inspections. Furthermore, misalignment of the grating with the rotation axis and deviations from ideal parallel illumination, as well as effects of the numerical filtering mentioned above might have an impact as well.

In order to verify the result, the grating structures in a 500 μm × 500 μm area were removed with a laser to allow height measurements. A stylus instrument was used to acquire a 700 μm line scan of the surface height across the hole. From this profile two measurements were derived: the height difference between the surrounding surface and the lowest point of the hole as well as the difference between the surrounding surface and the average height over the central 200 μm of the line scan. Figure 5 shows SEM images of the exposed area. It is apparent that the floor of the laser milled hole is inhomogeneous. At some positions the grating structures were not completely removed while at other positions parts of the substrate itself were removed. This lead to differences of up to 11 μm between the the two values, which can be seen as the inexactness in the height measurement.

The analysis with the stylus instrument yielded heights of 109 μm (maximal difference) and 105 μm (difference to the

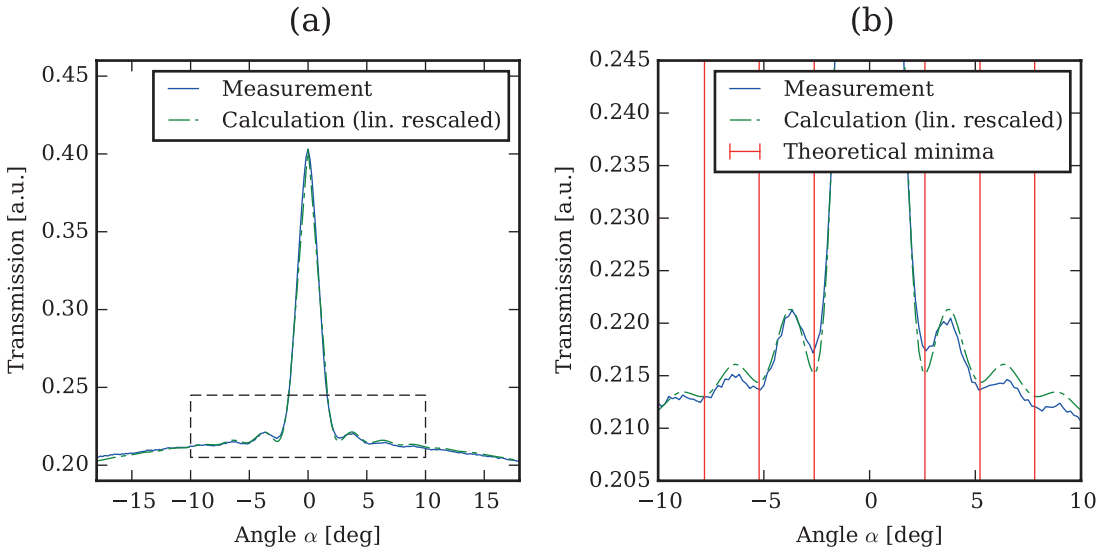

Figure 4. (a) Experimentally measured intensity curve in comparison with the calculated curve for the determined height of 106 μm. The *y*-axis of the theoretical curve was linearly rescaled. (b) shows the central portion of the left curve. The vertical lines show the theoretical minima positions according to the determined height of 106 μm and (2).

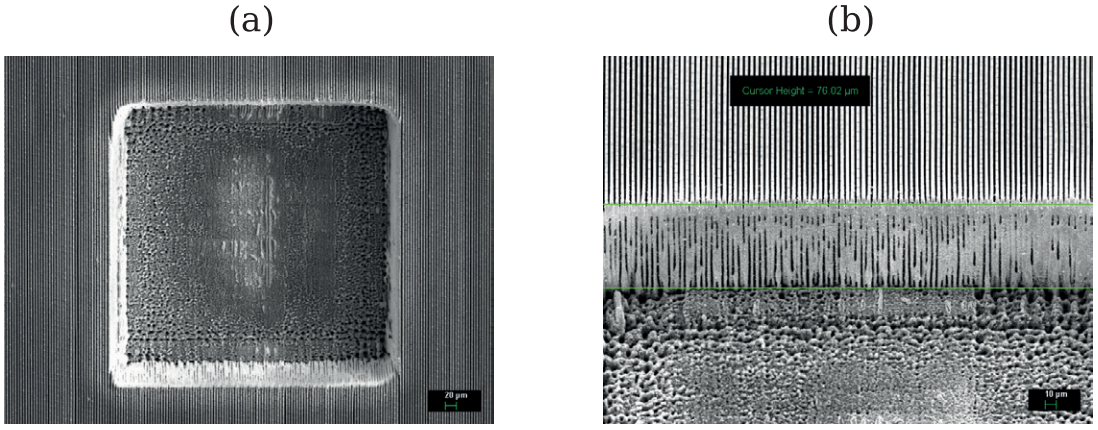

Figure 5. SEM images of a 500 μm × 500 μm hole, laser-milled at the position where the height was characterized. (a) Top-view of the hole. (b) The sidewall was tilted to appr. 45° and its height estimated to 108 μm.

central average). From the SEM image a height of 108 μm was estimated.

4. Discussion and conclusion

We presented a new method for characterizing the height of periodic structures using x-ray radiography. We demonstrated the feasibility of the approach on an x-ray absorption grating as is commonly used in x-ray phase-contrast imaging. By performing a rotation scan of the investigated structures under x-ray illumination, we could acquire an intensity curve that allowed the extraction of the structure height. The calculated heights are in good agreement with height measurements gained by destructive methods. Deviations are within the measurement tolerances of these methods.

A major advantage of our method is the ability to analyze the height without damaging the structures. The technique is therefore feasible for inspections of gratings that can be used for their primary application purpose.

The method furthermore does not rely on special equipment, e.g. high resolution detectors or micro focus sources, and can be carried out for example at the same setups at which the gratings are commonly used in. Therefore in most cases no additional hardware is required to apply the method. It is suitable for analyzing the height at specific points on the grating, for height homogeneity and quality control purposes.

With enhancements to the theoretical model, it might also be possible to directly fit the calculated curve to the measured data. This could further improve the accuracy of the height control, e.g. by eliminating possible position changes of asymmetric peaks during filtering. In addition it could allow the extraction of different grating parameters other than height. The duty cycle, for example influences the shape and position of the maxima in the intensity curve. Fitting the theoretical curve to those peaks might therefore yield additional information.

Future research has to focus on including the application of the approach to cone-beam geometry, which will

allow the spatially resolved control of heights over the whole grating area.

Acknowledgments

MS would like to thank the Helmholtz Virtual Institute for new x-ray analytic methods in material science (VI-NXMM) for the financial support of his studies. MS and FS would like to thank the TUM Graduate School. This work was carried out with the support of the Karlsruhe Nano Micro Facility (KNMF, www.knmf.kit.edu), a Helmholtz Research Infrastructure at Karlsruhe Institute of Technology (KIT, www.kit.edu). We acknowledge financial support through the DFG Cluster of Excellence Munich-Centre for Advanced Photonics (MAP), the DFG Gottfried Wilhelm Leibniz program and the support of the TUM Institute for Advanced Study, funded by the German Excellence Initiative.

References

[1] Pfeiffer F, Weitkamp T, Bunk O and David C 2006 *Nat. Phys.* **2** 258–61
[2] Pfeiffer F, Bech M, Bunk O, Kraft P, Eikenberry E F, Brönnimann C, Grünzweig C and David C 2008 *Nat. Mater.* **7** 134–7
[3] Weitkamp T, David C, Kottler C, Bunk O and Pfeiffer F 2006 *Proc. SPIE* **6318** 63180S
[4] Momose A 2003 *Opt. Express* **11** 2303–14
[5] Yang F, Prade F, Griffa M, Jerjen I, Di Bella C, Herzen J, Sarapata A, Pfeiffer F and Lura P 2014 *Appl. Phys. Lett.* **105** 154105
[6] Schleede S *et al* 2014 *Eur. J. Radiol.* **83** 531–6
[7] Pfeiffer F, Bunk O, David C, Bech M, Le Duc G, Bravin A and Cloetens P 2007 *Phys. Med. Biol.* **52** 6923–30
[8] Parsons D W, Morgan K, Donnelley M, Fouras A, Crosbie J, Williams I, Boucher R C, Uesugi K, Yagi N and Siu K K W 2008 *J. Anat.* **213** 217–27
[9] Donath T, Pfeiffer F, Bunk O, Grünzweig C, Hempel E, Popescu S, Vock P and David C 2010 *Investigative Radiol.* **45** 445–52
[10] Momose A, Yashiro W, Harasse S and Kuwabara H 2011 *Opt. Express* **19** 8423–32
[11] Wen H, Bennett E E, Hegedus M M and Rapacchi S 2009 *Radiology* **251** 910–8
[12] Velroyen A *et al* 2013 *Phys. Med. Biol.* **58** N37–46
[13] Yaroshenko A *et al* 2013 *Radiology* **269** 427–33
[14] Schaff F, Malecki A, Potdevin G, Eggl E, Noël P B, Baum T, Garcia E G, Bauer J S and Pfeiffer F 2014 *Sci. Rep.* **4** 3695
[15] David C, Bruder J, Rohbeck T, Grünzweig C, Kottler C, Diaz A, Bunk O and Pfeiffer F 2007 *Microelectron. Eng.* **84** 1172–7
[16] Becker E, Ehrfeld W, Hagmann P, Maner A and Münchmeyer D 1986 *Microelectron. Eng.* **4** 35–56
[17] Kenntner J, Altapova V, Grund T, Pantenburg F J, Meiser J, Baumbach T and Mohr J 2012 Fabrication and characterization of analyzer gratings with high aspect ratios for phase contrast imaging using a Talbot interferometer *Proc. of the 21st Int. AIP Congress* vol 1437 pp 89–93